Journal of Cardiovascular Magnetic Resonance (2006) **8,** 535–541

ISSN: 1097-6647 print / 1532-429X online
DOI: 10.1080/10976640600580296

Taylor & Francis
Taylor & Francis Group

MOLECULAR IMAGING AND NANOTECHNOLOGY

MR Three-Dimensional Molecular Imaging of Intramural Biomarkers with Targeted Nanoparticles

Tillmann Cyrus, MD, PhD,[1] Dana R. Abendschein, PhD,[1] Shelton D. Caruthers, PhD,[2] Thomas D. Harris, PhD,[3] Veronica Glattauer, PhD,[4] Jerome A. Werkmeister, PhD,[4] John A. M. Ramshaw, PhD,[4] Samuel A. Wickline, MD,[1] and Gregory M. Lanza, MD, PhD[1]

[1]Division of Cardiology, Washington University School of Medicine, Saint Louis, Missouri, USA
[2]Philips Medical Systems, Cleveland, Ohio, USA
[3]Bristol-Myers Squibb Medical Imaging, Billerica, Massachusetts, USA
[4]CSIRO, Victoria, Australia

ABSTRACT

In this study, porcine carotid arteries were subjected to balloon overstretch injury followed by local delivery of paramagnetic nanoparticles targeted to $\alpha_v\beta_3$-integrin expressed by smooth muscle cells or collagen III within the extracellular matrix. Carotid T_1-weighted angiography and vascular imaging was performed at 1.5T. While MR angiograms were indistinguishable between control and targeted vessel segments, $\alpha_v\beta_3$-integrin-and collagen III-targeted nanoparticles spatially delineated patterns and volumes of stretch injury. In conclusion, MR molecular imaging with $\alpha_v\beta_3$-integrin or collagen III-targeted nanoparticles enables the non-invasive, three-dimensional characterization of arterial pathology unanticipated from routine angiography.

INTRODUCTION

Magnetic resonance (MR) molecular imaging is emerging as an important technique for noninvasively assessing atherosclerotic vascular disease (1–3). While fluoroscopic-guided angiography and interventions are the dominant approaches used for revascularization, MRI–based techniques are in rapid development and beginning to gain acceptance. Angiographic approaches alone poorly define plaque pathology and do not delineate the extent of mural injury imparted by angioplasty. Despite marked improvements in revascularization techniques and devices, restenosis persists as a serious complication, which is at least partially dependent upon the inflammatory character of atherosclerotic plaque (4–14) and the impact of mechanical stress imparted by balloon injury (15, 16). MR molecular imaging probes infused locally into the balloon injured wall offer the potential to concomitantly delineate interventional injury patterns and characterize biochemical features exposed in the plaque at the time of intervention.

We have developed a lipid perfluorocarbon nanoparticle platform technology, which can be coupled to ligands and allows the specific targeting of biochemical epitopes (17). These nanoparticles are inherently echogenic (18) when bound to surfaces and can be modified for compatibility with MR (19), x-ray (20), or nuclear imaging (21). Ligand-targeted nanoparticles have been used for systemic vascular imaging of thrombosis (17) and angiogenesis (3, 22). Although nanoparticles are normally sterically precluded from reaching extravascular biomarkers, they can readily penetrate the vessel wall following stretch-injury. In prior experiments, tissue factor (TF) expressed by smooth muscle cells was targeted (23, 24), but unfortunately, the delay required for up regulation of TF on cell surfaces and a prolonged

Keywords: Magnetic Resonance Imaging, Molecular Imaging, Nanoparticles, Integrins, Collagen III, Angioplasty, Restenosis.
Received 4 September 2005; accepted 18 December 2005
The present research was conducted while Dr. T. Cyrus was a SCAI/Bracco Diagnostics, Inc.-ACIST Fellowship Program awardee. Additional funding and equipment were provided through National Institutes of Health grant support (HL-42950, HL-59865, HL-78631, NO1-CO-37007 and EB-01704), and the American Heart Association.
Correspondence to:
Gregory M. Lanza MD PhD
Washington University School of Medicine
660 South Euclid Ave., Campus Box 8086
Saint Louis, MO 63110
Tel. 314-454-8813
Fax. 314-454-5265
e-mail: greg@cmrl.wustl.edu
e-mail: tcyrus@cmrl.wustl.edu
Web: http://cmrl.wustl.edu

incubation used in those studies are incompatible with real-time phenotypic characterization and clinical application.

In this study, we evaluated the potential of ligand-targeted paramagnetic nanoparticles to detect $\alpha_v\beta_3$-integrin, constitutively expressed by smooth muscle cells or native collagen III within the extracellular matrix of carotid arteries immediately after balloon injury. Three-dimensional reconstruction was utilized to compare balloon injury patterns determined by molecular imaging of cellular versus extracellular epitopes. In addition, the relative intramural MR contrast enhancement achieved with the two molecular imaging targets was compared.

METHODS

Preparation of targeted nanoparticles

Ligand-targeted paramagnetic nanoparticles were prepared as previously described (17, 25). Briefly, the nanoparticles comprised 20% (volume/volume) perfluorooctylbromide (PFOB; Exfluor Research, Round Rock, TX, USA) and 1.5% (weight/volume) of a surfactant co-mixture, 1.7% (w/v) glycerin and water for the balance. The surfactant co-mixture included 69.9 mole% lecithin (Avanti Polar Lipids, Inc., Alabaster, AL, USA), 0.1 mole% peptidomimetic vitronectin antagonist (26–28) (Bristol-Myers Squibb Medical Imaging, Billerica, MA, USA) or anti-collagen III $f_{(ab)}$ (28, 29) (CSIRO, Victoria, Australia) coupled to MPB-PEG_{2000}-phosphatidylethanolamine (Northern Lipids, Inc., Vancouver, British Columbia, Canada), and 30 mole% of gadolinium diethylene-triamine-pentaacetic acid-bis-oleate (Gateway Chemical Technologies, St. Louis, MO, USA). Nontargeted, paramagnetic particles were prepared by substituting the ligand-lipid conjugate with lecithin. The nominal sizes for each formulation were measured with a submicron particle analyzer (Malvern Zetasizer, Malvern Instruments, Malvern, PA, USA) and were 245 nm $\pm$ 117 nm for the $\alpha_v\beta_3$-targeted, 262 nm $\pm$ 99 nm for the collagen III-targeted, and 323 nm $\pm$ 26 nm non-targeted control nanoparticles.

Preparation of targeted fluorescent nanoparticles

AlexaFluor 488-labeled nanoparticles were produced by inclusion of 0.5 mole% AlexaFluor 488 coupled to caproyl-phosphatidylethanolamine. AlexaFluor 488-caproyl-phosphatidylethanolamine was synthesized by dissolving 7.8 μmole AlexaFluor 488 carboxylic succinimidyl ester (Molecular Probes, Carlsbad, CA, USA) in 1.4 mL dimethylformamide and mixing it with 10 μmole caproylamine phosphatidylethanolamine (Avanti Polar Lipids, Alabaster, AL, USA) in 200 μL chloroform at 37°C for one hour. Following addition of 200 μL of chloroform, reaction temperature was increased to 50°C and continued overnight. TLC using a reverse phase hydrocarbon (C_{18}) impregnated silica gel and a mobile phase consisting of 0.1M sodium acetate buffer (pH5.6):methanol:water at a ratio of 20:100:200 was performed to monitor and purify the conjugated product from the uncoupled AlexaFluor dye. The red fluorescent lipid was recovered at the origin, extracted with chloroform:methanol (3:1) and evaporated to dryness until use.

Animal studies

All studies were approved by the Washington University Animal Studies Committee and are based on National Institutes of Health laboratory standards. Healthy domestic pigs weighing 20 kg were fed a normal diet (n = 12). Animals were fasted overnight before sedation with telazol cocktail (1 mL/23 kg IM) followed by intubation and 1–2% isoflurane anesthesia in oxygen. The ECG, blood gases and arterial blood pressure were monitored. A 12F (size necessary to fit the double-balloon catheter during incubation) catheter sheath was aseptically inserted into the femoral artery via a cut-down and a bolus of heparin (200 U/kg) was given to inhibit clot formation in catheters. No antiplatelet agents were administered. A guide catheter was placed under fluoroscopy into the left or right carotid artery at the level of the 5th cervical vertebra. A baseline carotid angiogram was obtained and lidocaine and nitroglycerin were used to treat vasospasm. An 8 mm $\times$ 2 cm balloon catheter (Proflex, Mallinckrodt Inc, St. Louis, MO, USA) was positioned at the level of the 2nd and 3rd cervical vertebrae and inflated three times to a pressure of 6 atmospheres for 30 seconds with 60 second pauses between inflations. A balloon-to-artery ratio of approximately 1.5 was employed. This procedure produces a consistent rupture of the internal elastic lamina and injury to the media (31, 32).

Following carotid overstretch-injury, nanoparticles were administered via a local delivery with a double-balloon catheter system (Edwards Lifesciences, Irvine, CA, USA). The 7F double balloon catheter was inserted via the sheath in the right femoral artery and guided into the respective carotid artery. The inner distance between the distal and the proximal balloons was 6 cm. Under fluoroscopy, the catheter was placed in a fashion that the injured vessel segment was positioned in the middle between the two balloons. The site of injury had been marked both on x-ray and on the overlying skin during the injury. Upon satisfactory confirmation of the double-balloon catheter position, the proximal and then distal balloons were each gently (1 atm) inflated to occlude the artery. Blood was aspirated through the central porthole, and the arterial segment flushed with normal saline. Targeted nanoparticles (n = 9 for $\alpha_v\beta_3$-integrin and n = 6 for collagen III) or non-targeted control nanoparticles (n = 3; into the contralateral artery), or saline alone as control (n = 6) were delivered locally and allowed to incubate for 10 minutes. The solutions were then withdrawn from the vessel and segment flushed thoroughly with saline before carotid flow was reestablished. A post-angioplasty carotid angiogram was obtained, and the animals were transferred for MR imaging of the neck vasculature.

Magnetic resonance imaging and NMR analysis

Animals were imaged with MRI using a 1.5 Tesla clinical scanner (NT Intera CV, Philips Medical Systems, Cleveland,

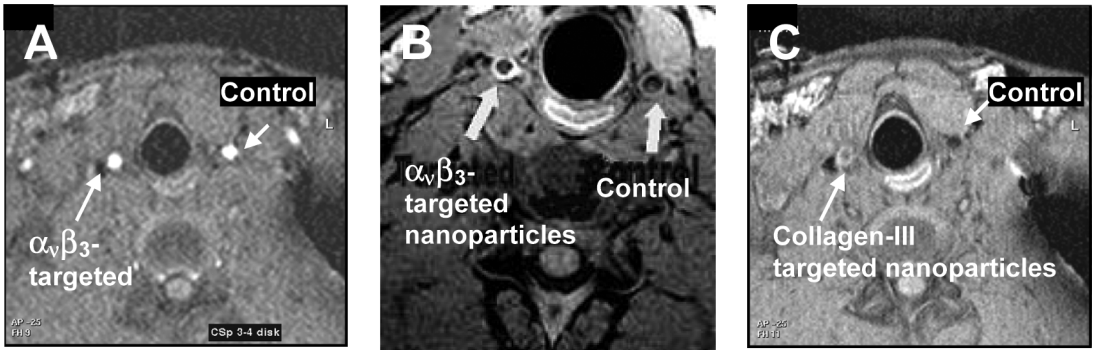

Figure 1. (A) Time-of-flight angiogram depicting blood flow in the carotid arteries of domestic pigs following balloon overstretch injury (femoral approach) and exposure to $\alpha_v\beta_3$-integrin targeted nanoparticles (left) or non-targeted nanoparticles as control (right). T_1-weighted black blood MR images of carotid arteries exposed for 10 minutes locally to paramagnetic nanoparticles covalently coupled to either (B) peptidomimetics targeted to $\alpha_v\beta_3$-integrin or (C) collagen III $F_{(ab)}$ fragments. T_1-weighted MRI at 1.5 T.

OH, USA) and techniques optimized to assess persistence of contrast enhancement and *in vivo* luminal dimensions throughout the injured vessels. A 5-element phased array surface coil operating in the receive mode was used. Multislice T_1-weighted, gradient-echo, fat-suppressed, time-of-flight angiograms of the carotid arteries from the carotid origin to the bifurcation into external and internal carotid were performed with repetition times (TR) of 40 ms and echo times (TE) of 4.6 ms. T_1-weighted, fat-suppressed, fast spin-echo (TSE) imaging was performed to image the vascular wall (TR = 532 ms, TE = 11 ms, 250 × 250 μm in-plane, 2 mm slice thickness, echo train = 4, number of signals averaged = 8). To ensure complete nulling of the blood signal, "sliding" radiofrequency saturation bands were placed proximal and distal to the region of image acquisition and moved with the selected imaging plane. Contrast to noise between the nanoparticles and surrounding tissue was calculated as the difference of the signal between the nanoparticle targeted area and a region of interest within the surrounding tissue, respectively, divided by the standard deviation of the background signal (33). Contrast image analysis was performed with Easy Vision v5.1 (Philips Medical Systems, Cleveland, OH, USA) using regions of interest manually applied in each slice of the T_1-weighted baseline images. The segmented slices were reconstructed into a three-dimensional object to calculate the volume.

Histology and immunohistology

Carotid vessels were excised for determination of arterial wall morphology and immunohistology. Frozen (OCT) segments from the injured vessels were sectioned every 7 microns and stained with hematoxylin and eosin (H&E), Masson's trichrome, Verhoeff-van Gieson for elastic tissue, and oil-red O for lipids. Microscopic images were obtained with a Nikon E800 microscope using a Nikon DXM 1200 digital camera connected to a Dell Dimension 4100 computer (Round Rock, TX) using Nikon ACT-1 image capture software (Nikon Inc., Melville, NY). Histomorphometric measurements of lumen, intima, media, and total vessel area were obtained. Immunohistology included detection of $\alpha_v\beta_3$−integrin (LM-609, Chemicon Int., Temecula, CA, USA) and collagen III (AB757P, Chemicon Int., Temecula, CA, USA). Vectastain Elite avidin-biotin complex method kits were used (Vector Laboratories, Burlingame, CA, USA).

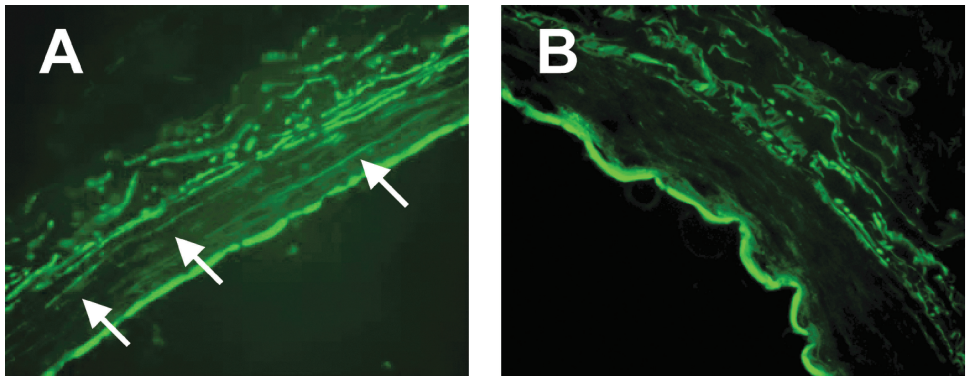

Figure 2. (A) $\alpha_v\beta_3$-integrin detected in the media after incubation with fluorescent PFC nanoparticles targeted against this integrin. (B) Exposure of contralateral artery to non-targeted PFC nanoparticles yields no specific immunofluorescence in the media. Both arteries exhibit auto-fluorescence in the adventitia and endothelium.

Statistical analysis

All quantitative data were analyzed with SAS (Cary, NC, USA) using general linear models and other descriptive statistics. Differences between means were declared significant at $p < 0.05$ and $b = 0.80$.

RESULTS

During MR scanning, T_1-weighted black blood images were obtained to evaluate vascular injury, and MR angiograms were obtained to assess luminal patency. No evidence of luminal narrowing was appreciated and time-of-flight carotid angiograms were indistinguishable between the targeted and contralateral control vessel segments (Fig. 1A). These results were consistent with X-ray contrast angiograms obtained immediately post procedure and before animal transfer to the MR suite.

Both biomarkers, collagen III and $\alpha_v\beta_3$-integrin, were exposed by stretch fracture of the carotid wall and were available immediately after injury for MR molecular imaging. The three dimensional contrast patterns established with collagen III and $\alpha_v\beta_3$-integrin molecular imaging were similar (Fig. 1B, C) and indicated that both biomarkers were generously distributed throughout the vessel wall. The resultant contrast pattern reflected the asymmetric pattern of injury imparted to the media and adventia by balloon overstretch shear forces, since the particles are otherwise sterically precluded from deep penetration into the extracellular matrix. Non-targeted nanoparticles and saline treatment produced no MR contrast enhancement and provided no information about the extent of mural injury. Successful targeting of intravascular epitopes was corroborated by histology using immunofluorescence in independent experiments where carotid arteries were incubated with fluorescent PFC nanoparticles targeted against the $\alpha_v\beta_3$-integrin (Fig. 2).

MR signal enhancement for the nanoparticle targeted vessel segments was intense and easily allowed for the determination of injury morphology. The contrast to noise ratio (CNR) between the $\alpha_v\beta_3$-integrin targeted nanoparticles and the surrounding arterial tissue measured with T_1-weighted, fat-suppressed, fast spin-echo (TSE) imaging was 13.8 ± 5.2, whereas the collagen III targeted nanoparticles provided a CNR of 3.3 ± 0.3 ($p < 0.05$; Fig. 3A). The difference in contrast presumably reflected the relative density of the biomarkers accessible to the nanoparticles within the wall and or differential probe avidity. The peptidomimetic ligand is small, with a molecular weight of ~1050 d, whereas the collagen III $f_{(ab)}$ fragment has a mass of approximately 50,000 d. As a result, the $\alpha_v\beta_3$-integrin nanoparticles presented 250 to 300 homing ligands per particle while the collagen III nanoparticles had 25 to 50 $f_{(ab)}$ fragments per particle. Clearly the $\alpha_v\beta_3$-integrin nanoparticles have a potential binding advantage that was minimized by locally infusing both nanoprobes at receptor-saturating concentrations.

The length of injury determined in all vascular segments exposed to $\alpha_v\beta_3$-integrin nanoparticles was $31 \text{ mm} \pm 5 \text{ mm}$, which was similar ($p > 0.05$) for the collagen III targeted carotids ($30 \text{ mm} \pm 4 \text{ mm}$). In both cases, the length of injury exceeded the actual balloon length (20 mm) by 50% (Fig. 3B). The absolute volume of vascular injury computed from the three-dimensional reconstructions of the contrast-segmented vessels did not differ ($p > 0.05$) between the $\alpha_v\beta_3$-targeted ($955 \text{ mm}^3 \pm 234 \text{ mm}^3$)

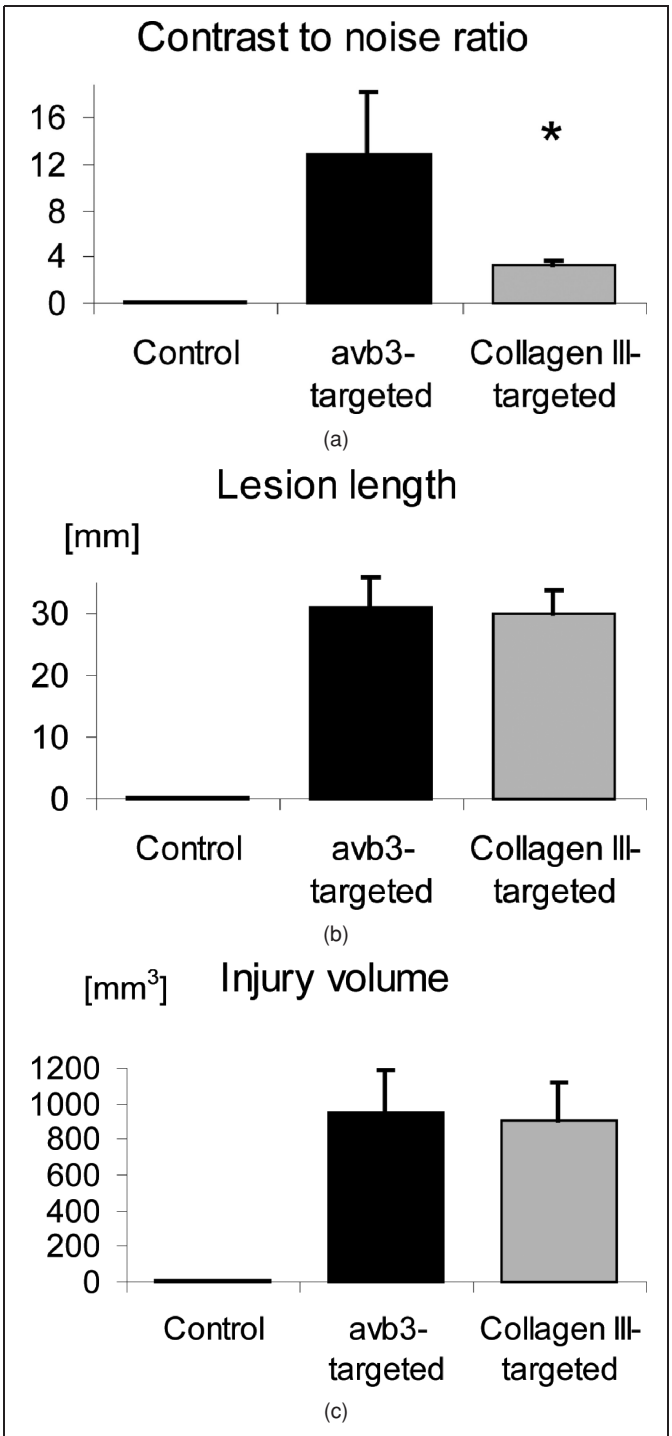

Figure 3. (A) Contrast to noise ratio for $\alpha_v\beta_3$-integrin and collagen III targeted nanoparticle emulsions (*$p < 0.05$). (B) Length of vascular injury as determined by MRI. (C) Quantitation of injury volume. T_1-weighted MRI at 1.5 T. None of the controls (vessels incubated with non-targeted nanoparticles or saline) displayed detectable signal for MR imaging.

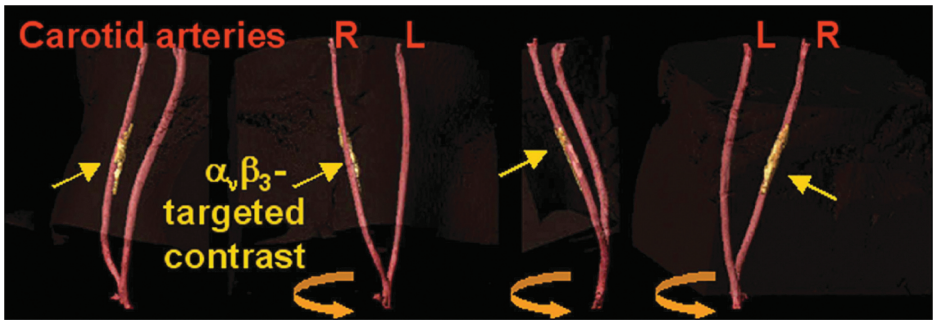

Figure 4. Volume-rendered image consisting of a 3-D MR angiogram co-registered with T_1 enhancement in the wall of carotid arteries of a domestic pig following angioplasty and exposure to $\alpha_v\beta_3$-targeted paramagnetic nanoparticles. Depiction of $\alpha_v\beta_3$-targeted contrast (golden; arrows) in the vascular wall. Frames at different angles detailing the asymetry and morphology of balloon overstretch injury pattern. MR angiography: TR 16 ms, TE 3.5 ms, a 60. MR vascular wall image: T_1-weighted MRI at 1.5 T, black-blood fast SE, TR 540 ms, TE 11 ms, a 90.

and collagen III targeted (903 mm^3 $\pm$ 218 mm^3) arteries (Fig. 3C).

Histology of the carotid arteries showed irregular loss of endothelium and disruptions in the media and internal elastic lamina propria as well as fractures reaching into the adventitia. Morphometric analyses from pigs treated with $\alpha_v\beta_3$-integrin targeted, collagen-III targeted, non-targeted nanoparticles, or saline were not significantly different. The presence and distribution of $\alpha_v\beta_3$-integrin and collagen III expression in the media were confirmed histologically (Fig. 5).

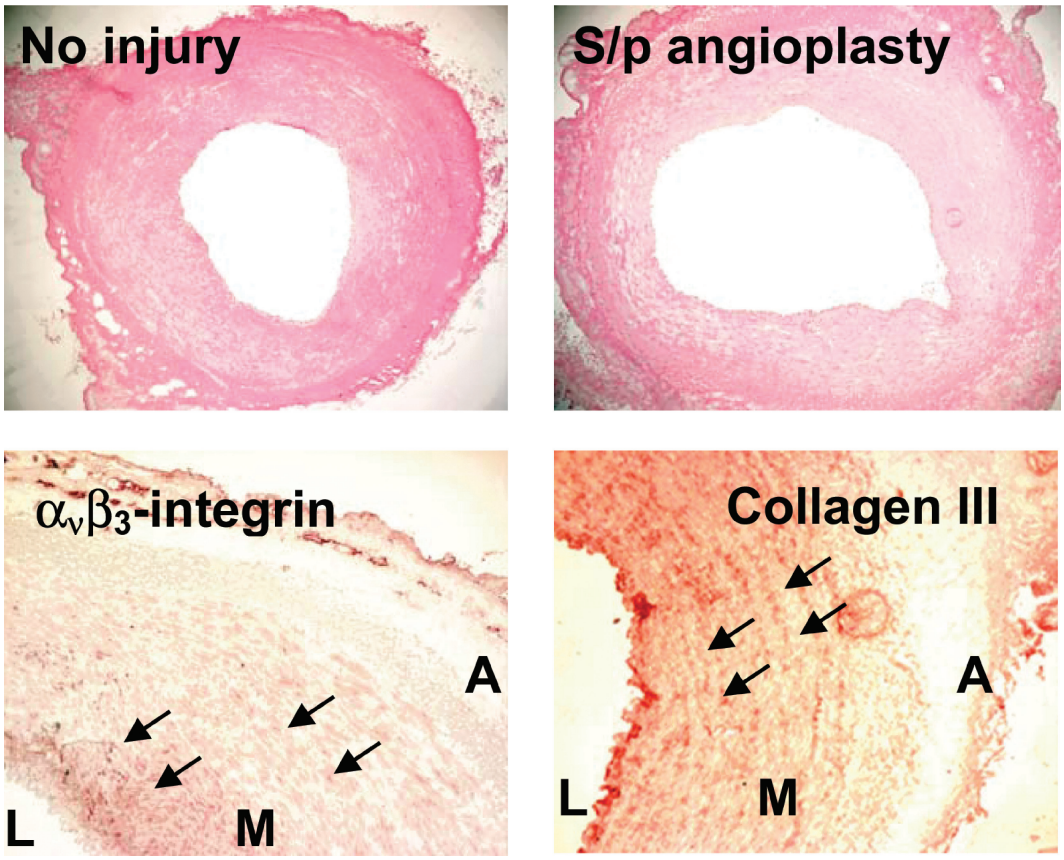

Figure 5. Representative cryosections from carotid arteries harvested immediately after MRI. Upper row: Hematoxylin eosin stains of uninjured versus balloon overstretch injured vessel. Lower row: $\alpha_v\beta_3$-integrin (LM-609) and collagen III (AB757P). S/p = status post, L = vascular lumen, M = media, A = adventitia, arrows point at molecular markers.

DISCUSSION

In the current experiments, we have established that paramagnetic nanoparticles can be used to target important biosignatures in the extracellular matrix or expressed on cell surfaces following balloon overstretch injury. In contrast to conventional angiography, which delineates vascular filling defects, these nanoparticles are capable of infiltrating the vessel wall through the fissures created by balloon overstretch injury and then binding to epitopes within the vessel wall thereby delineating the wall morphology. This unique MR-based technology could permit in situ physiological characterization of atherosclerotic plaques immediately after injury, which may facilitate individualized therapy decisions based on injured plaque pathology.

In the present study, we sought to establish the feasibility of targeting two types of epitopes (extracellular vs. cell membrane) and to compare their efficacy. Both the extracellular matrix target collagen III and the smooth muscle cell membrane epitope $\alpha_v\beta_3$-integrin were generously distributed and bioavailable for binding. Interestingly, the $\alpha_v\beta_3$-integrin targeted nanoparticles produced a four-fold greater contrast signal relative to the wall than the collagen III targeted agent. This suggests a higher retention of the integrin-targeted agent, which may be due in part to differences in the number of binding sites exposed or available to the particulate probe. Although the surface presentation of ligands varied considerably between the two formulations due to molecular weight differences, it is likely that this effect was minimized by administering saturating concentrations of nanoparticles into the wall.

Importantly, despite the difference in contrast signal relative to wall, both nanoparticle formulations provided adequate image quality, and there was no difference in the ability to analyze lesion length, three-dimensional geometry, and volume. Thus, both collagen III targeted and $\alpha_v\beta_3$-integrin targeted nanoparticles equivalently delineated vascular wall stretch-injury patterns. These data illustrate the ability of MR molecular imaging probes to supplement the characterization of vascular pathology beyond luminal dimensions with biochemical and mechanical injury data in a timely fashion. An incubation time of 10 minutes was chosen in the current study to achieve adequate exposure of injured media to the nanoparticle emulsion. In the future, delivery devices such as porous balloons may be chosen to minimize or eliminate vascular occlusion times while delivering the nanoparticles into the injured vascular wall.

Despite major advancements afforded by drug-eluting stents, a significant subset of patients and lesions remain in which restenosis or thrombosis is still prevalent. The potential to develop clinical restenosis after vascular injury is influenced by the mechanical shear forces of angioplasty and the underlying biochemical character of the atheroma. Many investigators have demonstrated the influence of mechanical shear force created by balloon injury on the stimulation of biochemical and intracellular signaling processes, which contribute to restenosis (8, 13, 15, 34). Recurrent unstable angina and restenosis may also depend upon the overall inflammatory status of the plaque, which can vary considerably among lesions and patients. Histological analysis of coronary plaque atherectomy specimens have demonstrated that increased atheroma inflammation, suggested by larger infiltrations of macrophages and T-cells, was related to recurrent unstable angina and that the concentration of macrophages was an independent predictor of restenosis (8). Ligand-directed paramagnetic nanoparticles may allow real-time pathologic characterization of the injured atheroma, which could be predictive of recurrent symptoms after angioplasty and may provide a convenient drug-delivery vehicle for individualized therapy (35).

CONCLUSION

In contradistinction to conventional angiograms, which delineate patency of vasculature, MR molecular imaging nanoparticles provide an assessment of the spatial distribution of both cell surface and extracellular matrix biomarkers. The quantitative measurements of three-dimensional balloon injury pattern and the prevalence of pathologic biomarkers may provide prognostic information at the time of intervention undetectable today. MR molecular imaging could reveal unique assessments and allow individualized revascularization strategies.

ACKNOWLEDGEMENTS

We are grateful for the expert technical assistance by John S. Allen, BS, and Todd A. Williams, BS. We also appreciate the support and helpful discussions with Thomas D. Harris, PhD, Bristol-Myers Squibb Medical Imaging, Billerica, MA.

REFERENCES

1. Kooi ME, Cappendijk VC, Cleutjens KBJM, Kessels AGH, Kitslaar PJEHM, Borgers M, Frederik PM, Daemen MJAP, van Engelshoven JMA. Accumulation of ultrasmall superparamagnetic particles of iron oxide in human atherosclerotic plaques can be detected by in vivo magnetic resonance imaging. Circulation 2003;107:2453–8.
2. Ruehm SG, Corot C, Vogt P, Kolb S, Debatin JF. Magnetic resonance imaging of atherosclerotic plaque with ultrasmall superparamagnetic particles of iron oxide in hyperlipidemic rabbits. Circulation 2001;103:415–22.
3. Winter PM, Morawski AM, Caruthers SD, Fuhrhop RW, Zhang H, Williams TA, Allen JS, Lacy EK, Robertson JD, Lanza GM, Wickline SA. Molecular imaging of angiogenesis in early-stage atherosclerosis with $\alpha_v\beta_3$-integrin-targeted nanoparticles. Circulation 2003;108:2270–4.
4. Buffon A, Liuzzo G, Biasucci LM, Pasqualetti P, Ramazzotti V, Rebuzzi AG, Crea F, Maseri A. Preprocedural serum levels of C-reactive protein predict early complications and late restenosis after coronary angioplasty. Journal of the American College of Cardiology 1999;34:1512–21.
5. Danenberg HD, Szalai AJ, Swaminathan RV, Peng L, Chen Z, Seifert P, Fay WP, Simon DI, Edelman ER. Increased thrombosis after arterial injury in human C-reactive protein-transgenic mice. Circulation 2003;108:512–5.
6. Dibra A, Mehilli J, Braun S, Hadamitzky M, Baum H, Dirschinger J, Schuhlen H, Schomig A, Kastrati A. Association between

C-reactive protein levels and subsequent cardiac events among patients with stable angina treated with coronary artery stenting. The American Journal of Medicine 2003;114:715–22.
7. Liuzzo G, Buffon A, Biasucci LM, Gallimore JR, Caligiuri G, Vitelli A, Altamura S, Ciliberto G, Rebuzzi AG, Crea F, et al. Enhanced inflammatory response to coronary angioplasty in patients with severe unstable angina. Circulation 1998;98:2370–76.
8. Meuwissen M, Piek JJ, van der Wal AC, Chamuleau SAJ, Koch KT, Teeling P, van der Loos CM, Tijssen JGP, Becker AE. Recurrent unstable angina after directional coronary atherectomy is related to the extent of initial coronary plaque inflammation. Journal of the American College of Cardiology 2001;37:1271–6.
9. Patti G, Di Sciascio G, D'Ambrosio A, Dicuonzo G, Abbate A, Dobrina A. Prognostic value of interleukin-1 receptor antagonist in patients undergoing percutaneous coronary intervention. The American Journal of Cardiology 2002;89:372–6.
10. Pietersma A, Kofflard M, Wit LEAD, Stijnen T, Koster JF, Serruys PW, Sluiter W. Late lumen loss after coronary angioplasty is associated with the activation status of circulating phagocytes before treatment. Circulation 1995;91:1320–5.
11. Rahel BM, Visseren FLJ, Suttorp MJ, Plokker THW, Kelder JC, de Jongh BM, Bouter KP, Diepersloot RJA. Preprocedural serum levels of acute-phase reactants and prognosis after percutaneous coronary intervention. Cardiovascular Research 2003;60:136–40.
12. Stefanadis C, Toutouzas K, Tsiamis E, Stratos C, Vavuranakis M, Kallikazaros I, Panagiotakos D, Toutouzas P. Increased local temperature in human coronary atherosclerotic plaques: An independent predictor of clinical outcome in patients undergoing a percutaneous coronary intervention. Journal of the American College of Cardiology 2001;37:1277–83.
13. Toutouzas K, Colombo A, Stefanadis C. Inflammation and restenosis after percutaneous coronary interventions. Eur Heart J 2004;25:1679–87.
14. Walter D H, Fichtlscherer S, Sellwig M, Auch-Schwelk W, Schachinger V, Zeiher AM. Preprocedural C-reactive protein levels and cardiovascular events after coronary stent implantation. Journal of the American College of Cardiology 2001;37:839–46.
15. Li L, Couse TL, Deleon H, Xu CP, Wilcox JN, Chaikof EL. Regulation of syndecan-4 expression with mechanical stress during the development of angioplasty-induced intimal thickening. Journal of Vascular Surgery 2002;36:361–70.
16. Wentzel JJ, Kloet J, Andhyiswara I, Oomen JAF, Schuurbiers JCH, de Smet BJGL, Post MJ, de Kleijn D, Pasterkamp G, Borst C, et al., Shear-stress and wall-stress regulation of vascular remodeling after balloon angioplasty: Effect of matrix metalloproteinase inhibition. Circulation 2001;104:91–6.
17. Lanza GM, Wallace KD, Scott MJ, Cacheris WP, Abendschein DR, Christy DH, Sharkey AM, Miller JG, Gaffney PJ, Wickline SA. A novel site-targeted ultrasonic contrast agent with broad biomedical application. Circulation 1996;94:3334–40.
18. Lanza GM, Trousil RL, Wallace KD, Rose JH, Hall CS, Scott MJ, Miller JG, Eisenberg PR, Gaffney PJ, Wickline SA. In vitro characterization of a novel, tissue-targeted ultrasonic contrast system with acoustic microscopy. J Acoust Soc Am 1998;104:3665–72.
19. Lanza GM, Lorenz CH, Fischer SE, Scott MJ, Cacheris WP, Kaufmann RJ, Gaffney PJ, Wickline SA. Enhanced detection of thrombi with a novel fibrin-targeted magnetic resonance imaging agent. Academic Radiology 1998;5:S173–S176.
20. Winter PM, Shukla HP, Caruthers SD, Scott MJ, Fuhrhop RW, Robertson JD, Gaffney PJ, Wickline SA, Lanza GM. Molecular imaging of human thrombus with computed tomography. Academic Radiology 2005;12:9–13.
21. Lanza GM, Wickline SA, Inventors, and Barnes-Jewish Hospital. Site specific binding system, nuclear imaging compositions and methods. US patent 5,958,371 09/28/1999.
22. Winter PM, Caruthers SD, Kassner A, Harris TD, Chinen LK, Allen JS, Lacy EK, Zhang H, Robertson JD, Wickline SA, Lanza GM. Molecular imaging of angiogenesis in nascent vx-2 rabbit tumors using a novel $\alpha_v\beta_3$-targeted nanoparticle and 1.5 tesla magnetic resonance imaging. Cancer Res 2003;63:5838–43.
23. Lanza GM, Abendschein DR, Hall CS, Marsh JN, Scott MJ, Scherrer DE, Wickline SA. Molecular imaging of stretch-induced tissue factor expression in carotid arteries with intravascular ultrasound. Investigative Radiology 2000;35:227–34.
24. Lanza GM, Abendschein DR, Hall CS, Scott MJ, Scherrer DE, Houseman A, Miller JG, Wickline SA. In vivo molecular imaging of stretch-induced tissue factor in carotid arteries with ligand-targeted nanoparticles. Journal of the American Society of Echocardiography 2000;13:608–14.
25. Flacke S, Fischer S, Scott MJ, Fuhrhop RJ, Allen JS, McLean M, Winter P, Sicard GA, Gaffney PJ, Wickline SA, Lanza GM. Novel MRI contrast agent for molecular imaging of fibrin: Implications for detecting vulnerable plaques. Circulation 2001;104:1280–5.
26. Harris TD, Kalogeropoulos S, Nguyen T, Liu S, Bartis J, Ellars C, Edwards S, Onthank D, Silva P, Yalamanchili P, et al. Design, synthesis, and evaluation of radiolabeled integrin alpha v beta 3 receptor antagonists for tumor imaging and radiotherapy. Cancer Biotherapy & Radiopharmaceuticals 2003;18:627–41.
27. Meoli DF, Sadeghi MM, Krassilnikova S, Bourke BN, Giordano FJ, Dione DP, Su H, Edwards DS, Liu S, Harris TD, et al. Noninvasive imaging of myocardial angiogenesis following experimental myocardial infarction. J Clin Invest 2004;113:1684–91.
28. Sadeghi MM, Krassilnikova S, Zhang J, Gharaei A A, Fassaei HR, Esmailzadeh L, Kooshkabadi A, Edwards S, Yalamanchili P, Harris TD, et al. Detection of injury-induced vascular remodeling by targeting activated $\alpha_v\beta_3$-integrin in vivo. Circulation 2004;110:84–90.
29. Glattauer V, Werkmeister JA, Kirkpatrick A, Ramshaw JAM. Identification of the epitope for a monoclonal antibody that blocks platelet aggregation induced by type III collagen. Biochemical Journal 1997;323:45–9.
30. Werkmeister JA, Ramshaw JA. Multiple antigenic determinants on type III collagen. Biochemical Journal 1991;274:895–8.
31. Recchia D, Abendschein DR, Saffitz JE, Wickline SA. The biologic behavior of balloon hyperinflation-induced arterial lesions in hypercholesterolemic pigs depends on the presence of foam cells. Arteriosclerosis Thrombosis and Vascular Biology 1995;15:924–9.
32. Steele PM, Chesebro JH, Stanson AW, Holmes DRJ, Dewanjee MK, Badimon L, Fuster V. Balloon angioplasty. Natural history of the pathophysiological response to injury in a pig model. Circulation Research 1985;57:105–12.
33. Henkelman R. Measurement of signal intensities in the presence of noise in MR images. Medical Physics 1985;12:232–3.
34. Miketíc SA, Carlsson J, Tebbe U. Influence of gradually increased slow balloon inflation on restenosis after coronary angioplasty. American Heart Journal 1998;135:709–13.
35. Lanza GM, Yu X, Winter PM, Abendschein DR, Karukstis KK, Scott MJ, Chinen LK, Fuhrhop RW, Scherrer DE, Wickline SA. Targeted antiproliferative drug delivery to vascular smooth muscle cells with a magnetic resonance imaging nanoparticle contrast agent: Implications for rational therapy of restenosis. Circulation 2002;106:2842–7.